Supplementary Information

Cr-Zn/Ni-Containing Nanocomposites as Effective Magnetically Recoverable Catalysts for CO_2 Hydrogenation to Methanol: The Role of Metal Doping and Polymer Co-Support.

Svetlana A. Sorokina [1], Nina V. Kuchkina [1], Maxim E. Grigoriev [2], Alexey V. Bykov [2], Andrey K. Ratnikov [1], Valentin Yu. Doluda [2], Mikhail G. Sulman [2] and Zinaida B. Shifrina [1,*]

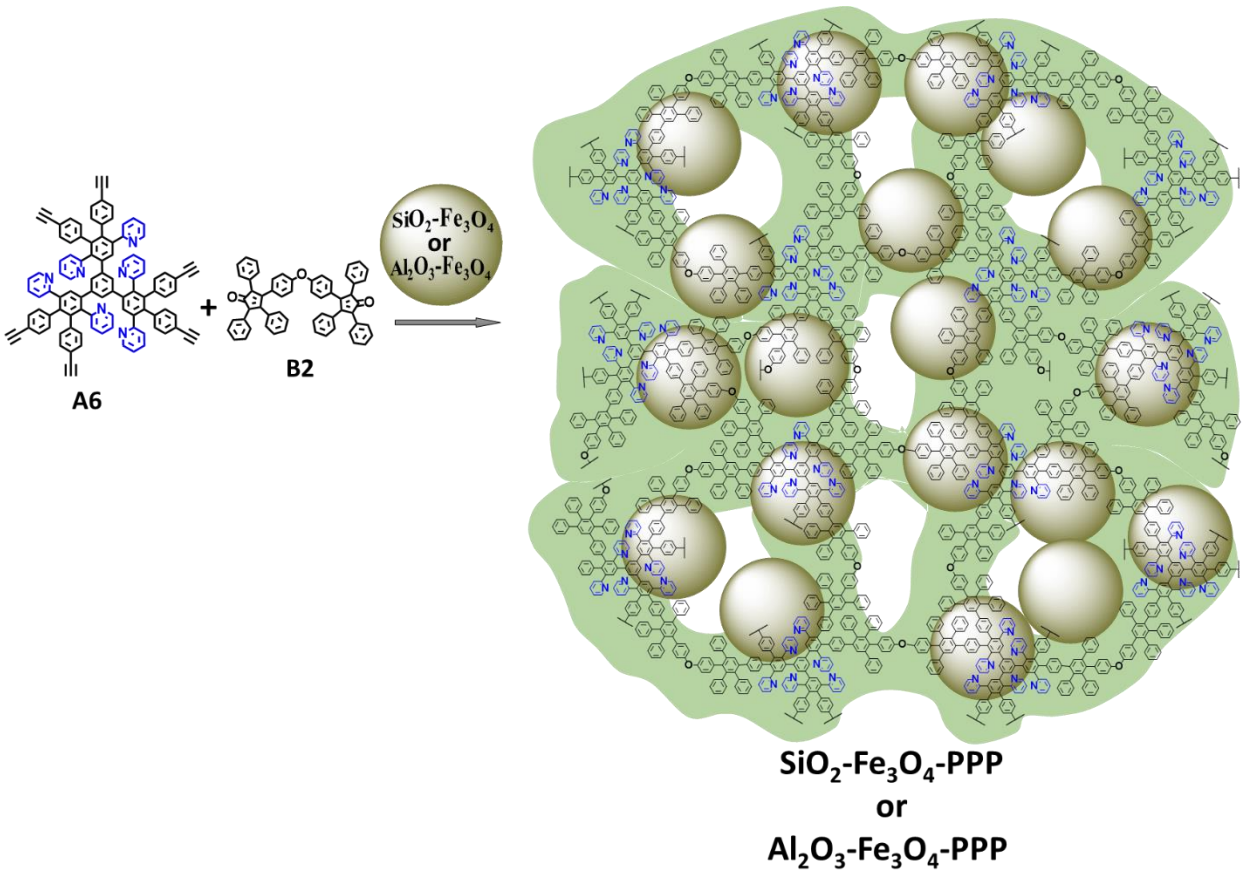

Figure S1. Schematic presentation of deposition of a thin layer of pyridylphenylene polymer on a solid support.

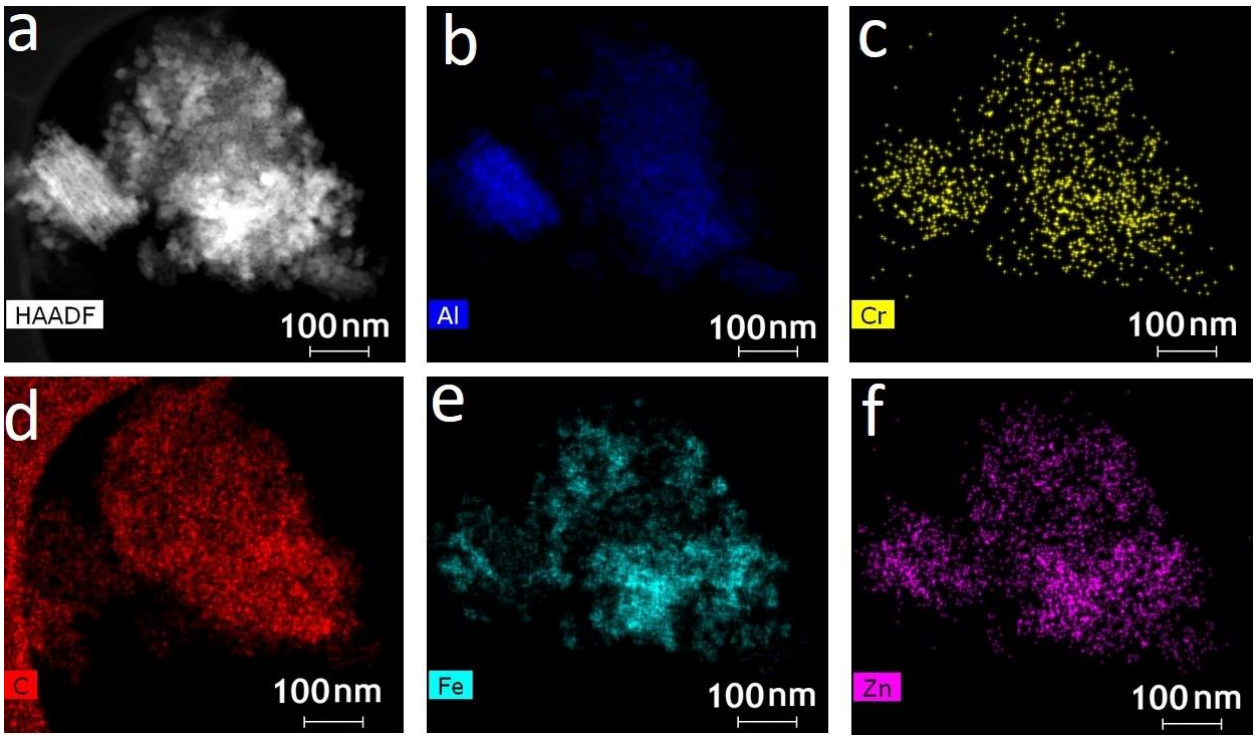

Figure S2. STEM EDS maps of Al_2O_3-Fe_3O_4-PPP-Cr-Zn

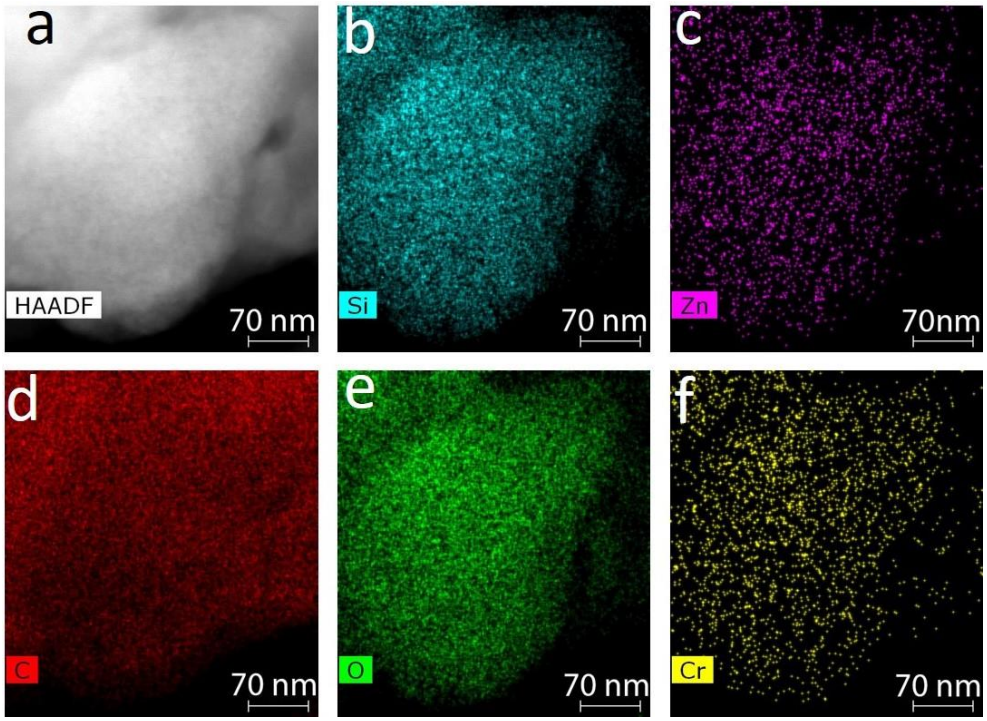

Figure S3. STEM EDS maps of SiO_2-PPP-Cr-Zn

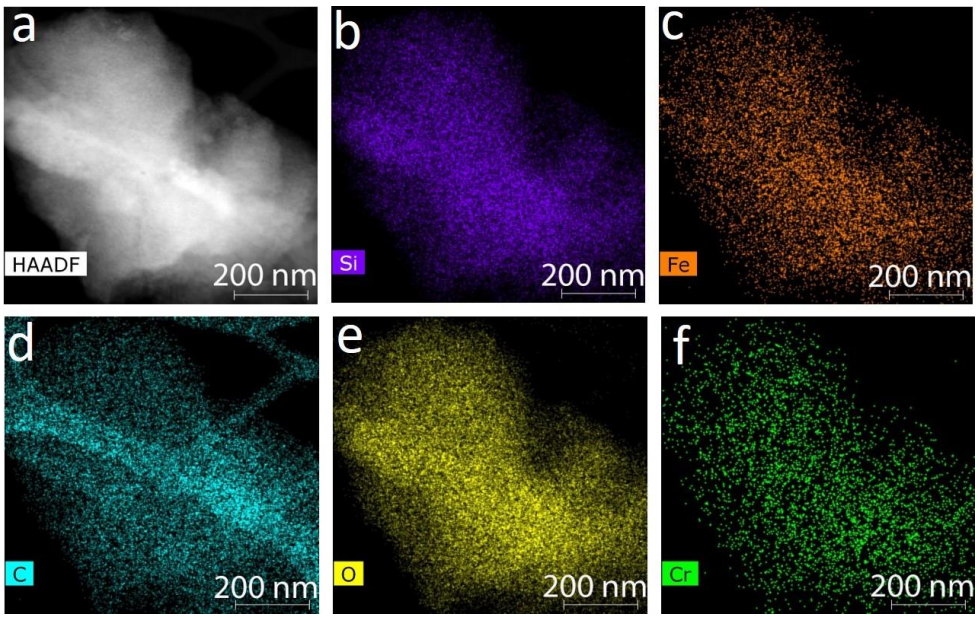

Figure S4. STEM EDS maps of SiO_2-Fe_3O_4-PPP-Cr

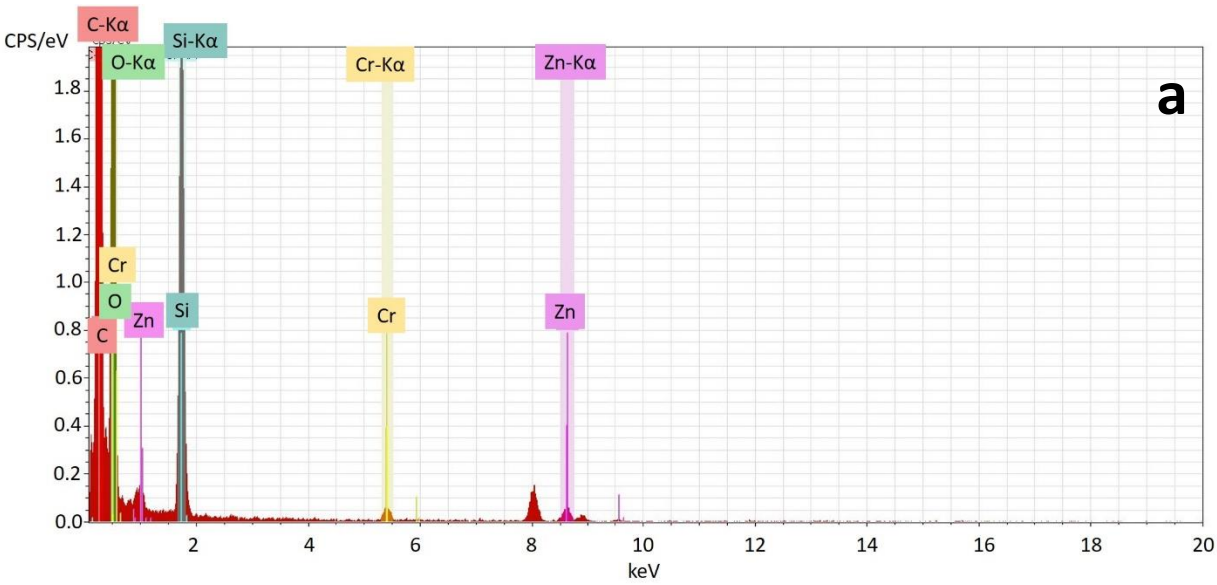

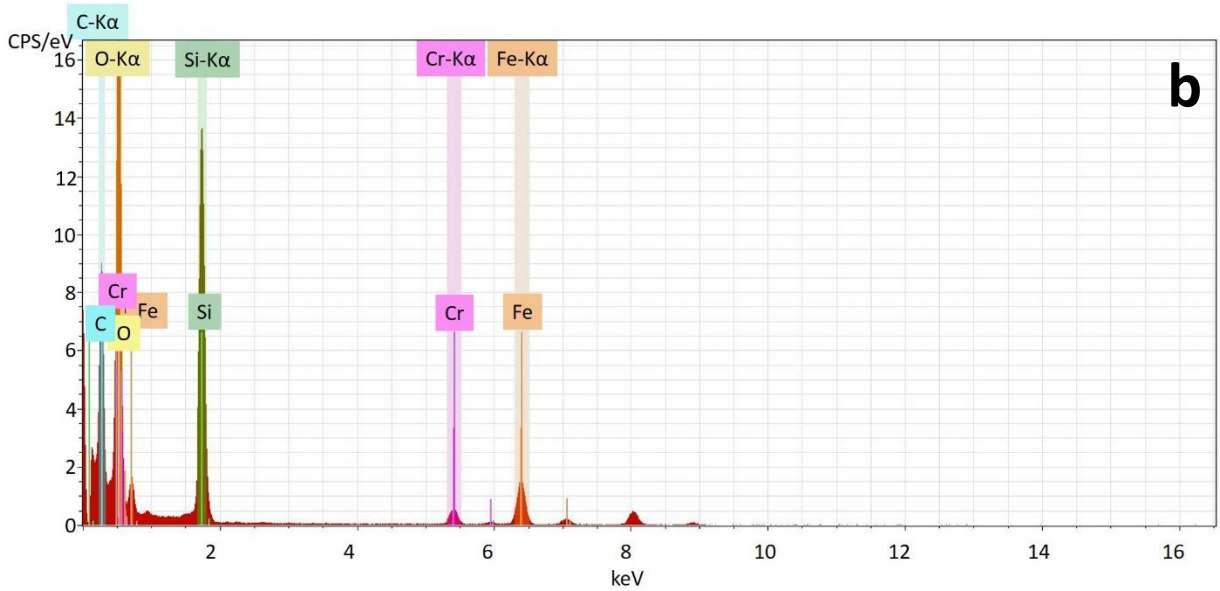

Figure S5. EDS spectra of SiO_2-PPP-Cr-Zn (a) and SiO_2-Fe_3O_4-PPP-Cr (b) nanocomposites.

Table S1. Atomic percentage of elements in samples.

Sample	Atomic %							Total
	C	Si/Al*	O	Fe	Cr	Zn	Ni	
SiO_2-Fe_3O_4-PPP-Cr-Zn	38.43	22.74	36.75	1.24	0.43	0.41	0	100
SiO_2-Fe_3O_4-PPP-Cr	63.51	11.77	22.86	1.47	0.39	0	0	100
SiO_2-Fe_3O_4-PPP-Cr-Ni	57.99	15.10	24.72	1.30	0.56	0	0.33	100
SiO_2-PPP-Cr-Zn	60.31	17.30	21.56	0	0.41	0.42	0	100
Al_2O_3-Fe_3O_4-PPP-Cr-Zn*	58.99	12.96	22.80	4.38	0.44	0.43	0	100

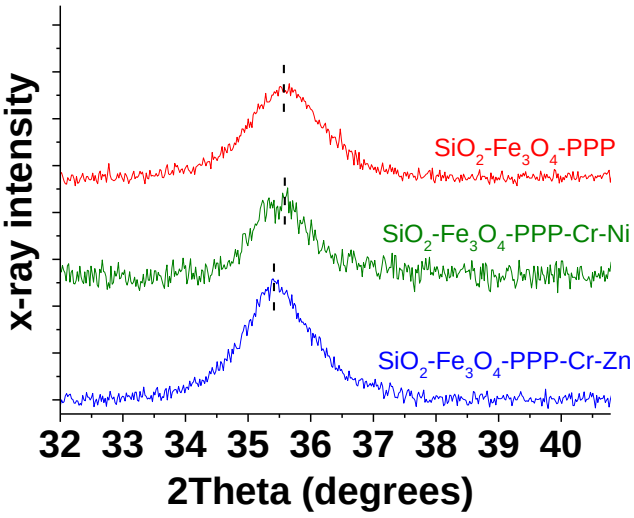

Figure S6. XRD patterns of the samples in the area of the (311) spinel peak.

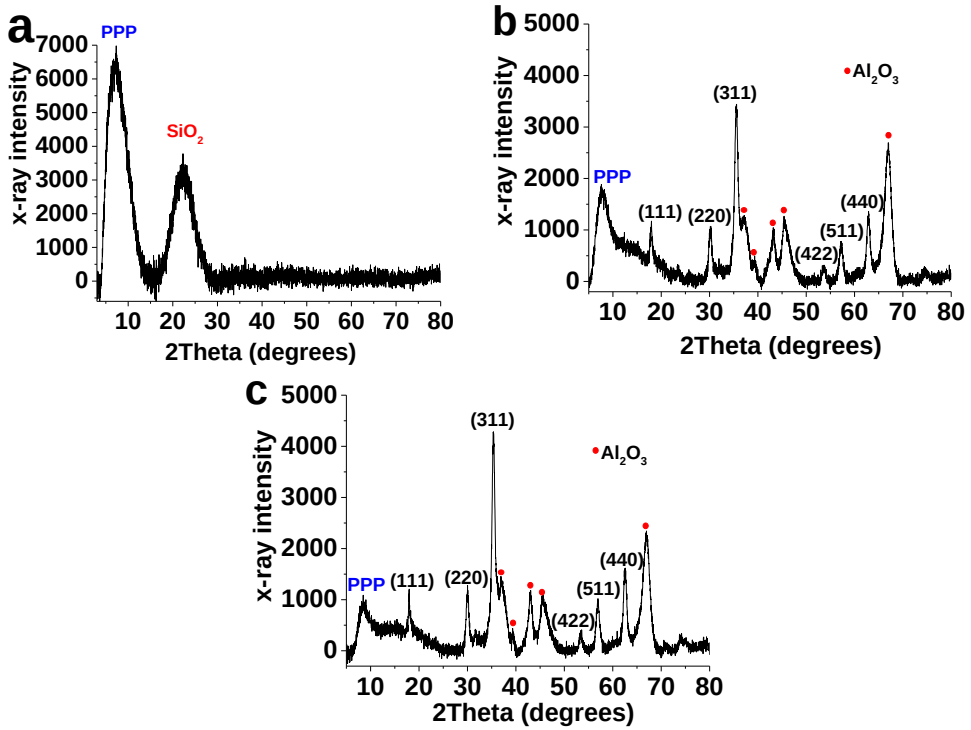

Figure S7. XRD patterns of SiO_2-PPP-Cr-Zn (a), Al_2O_3-Fe_3O_4-PPP (b), Al_2O_3-Fe_3O_4-PPP-Cr-Zn (c)

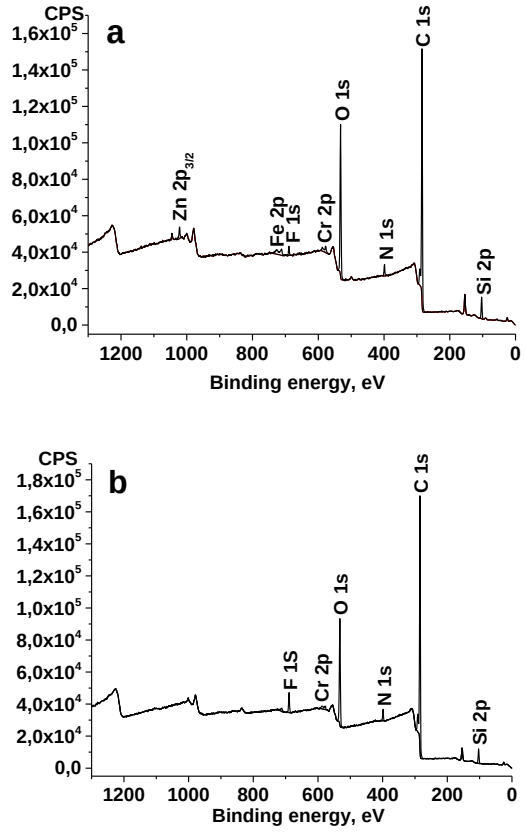

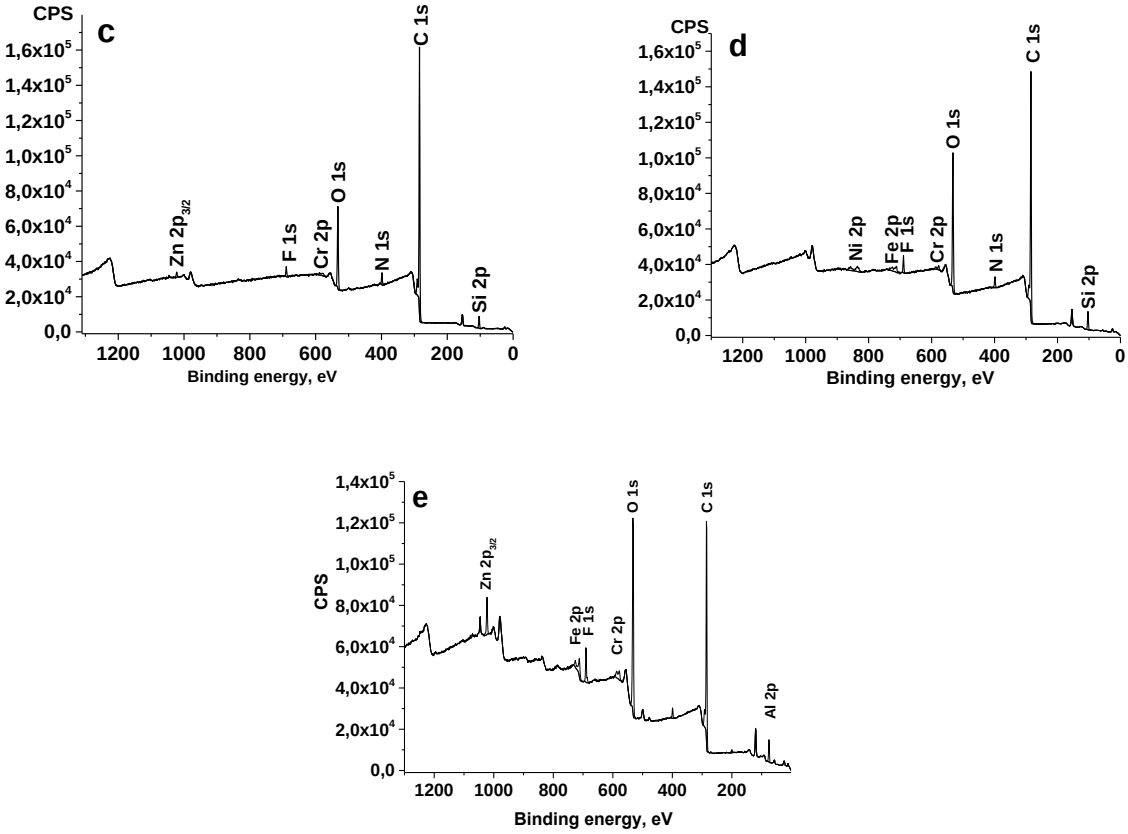

Figure S8. XPS survey spectra of the SiO_2-Fe_3O_4-PPP-Cr-Zn (a), SiO_2-Fe_3O_4-PPP-Cr (b), SiO_2-PPP-Cr-Zn (c), SiO_2-Fe_3O_4-PPP-Cr-Ni (d), Al_2O_3-Fe_3O_4-PPP-Cr-Zn (e) nanocomposites.

Table S2. Fitting parameters for HR XPS of Fe 2p, Cr 2p and Zn 2p of SiO_2-Fe_3O_4-PPP-Cr-Zn.

Band	Position, eV	FWHM, eV	%Area
Fe			
1	711.00	2.66	11.67
2	712.20	4.03	23.34
3	715.00	4.74	12.61
4	719.90	7.18	19.05
5	724.60	2.66	5.83
6	725.80	4.03	11.67
7	728.60	4.74	6.30
8	733.50	7.18	9.53
Zn			
1	1022.50	1.98	64.26

2	1045.60	2.28	35.74
Cr			
1	573.00	5.00	8.50
2	577.38	2.51	48.25
3	585.18	5.38	12.25
4	587.25	2.51	24.12
5	595.00	10.00	2.96
6	599.60	5.10	3.91

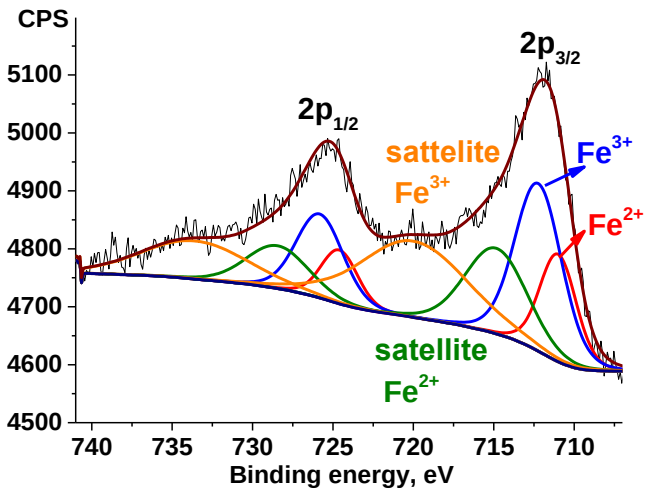

Figure S9. HR XPS of Fe 2p of SiO_2-Fe_3O_4-PPP before incorporation of metal oxides in the nanocomposite structure.

Table S3. Fitting parameters for HR XPS of Fe 2p of SiO_2-Fe_3O_4-PPP.

Band	Position, eV	FWHM, eV	% Area
1	711.00	2.69	10.41
2	712.23	3.45	20.81
3	714.86	4.54	13.99
4	720.01	7.81	21.45
5	724.60	2.69	5.20
6	725.83	3.45	10.41
7	728.46	4.54	7.00
8	733.61	7.81	10.73

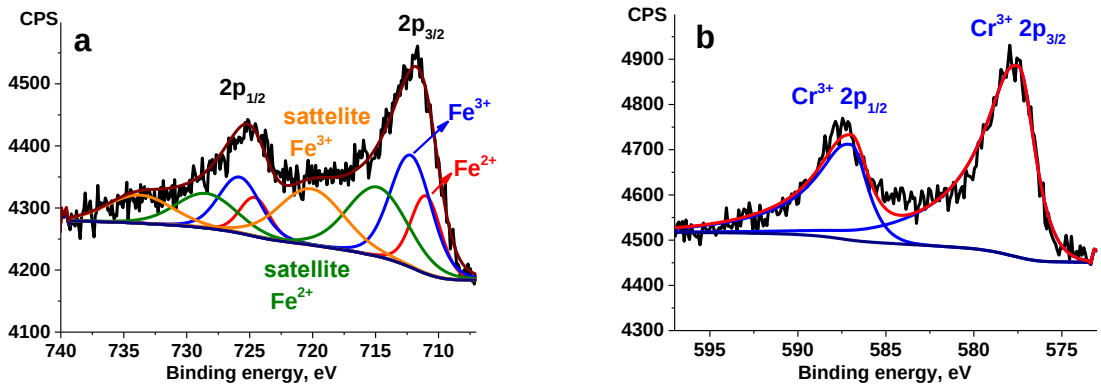

Figure S10. HR XPS of Fe 2p (a) and Cr 2p (b) regions of SiO_2-Fe_3O_4-PPP-Cr

Table S4. Fitting parameters for HR XPS of Fe 2p and Cr 2p of SiO_2-Fe_3O_4-PPP-Cr.

Band	Position, eV	FWHM, eV	%Area
Fe			
1	711.00	2.79	10.44
2	712.20	3.88	20.88
3	714.84	5.66	18.84
4	720.10	6.11	16.51
5	724.60	2.79	5.22
6	725.80	3.88	10.44
7	728.44	5.66	9.42
8	733.70	6.11	8.25
Cr			
1	577.47	2.22	66.67
2	586.98	2.22	33.33

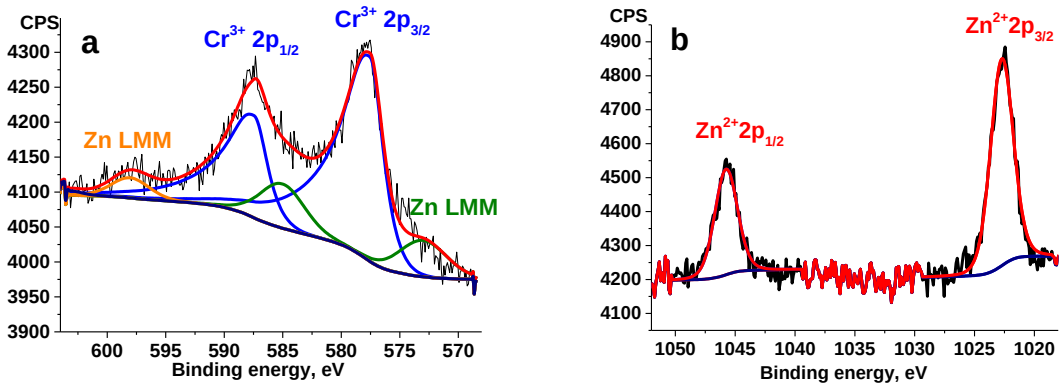

Figure S11. HR XPS of Cr 2p (a) and Zn 2p (b) regions of SiO_2-PPP-Cr-Zn

Table S5. Fitting parameters for HR XPS Cr 2p and Zn 2p of SiO_2-PPP-Cr-Zn

Band	Position, eV	FWHM, eV	%Area
Cr			
1	573.00	4.74	8.42
2	577.56	2.69	51.71
3	585.05	4.50	9.72
4	587.45	2.69	25.86
5	598.04	3.83	3.76
6	603.22	2.56	0.53
Zn			
1	1022.71	2.23	66.10
2	1045.76	2.24	33.90

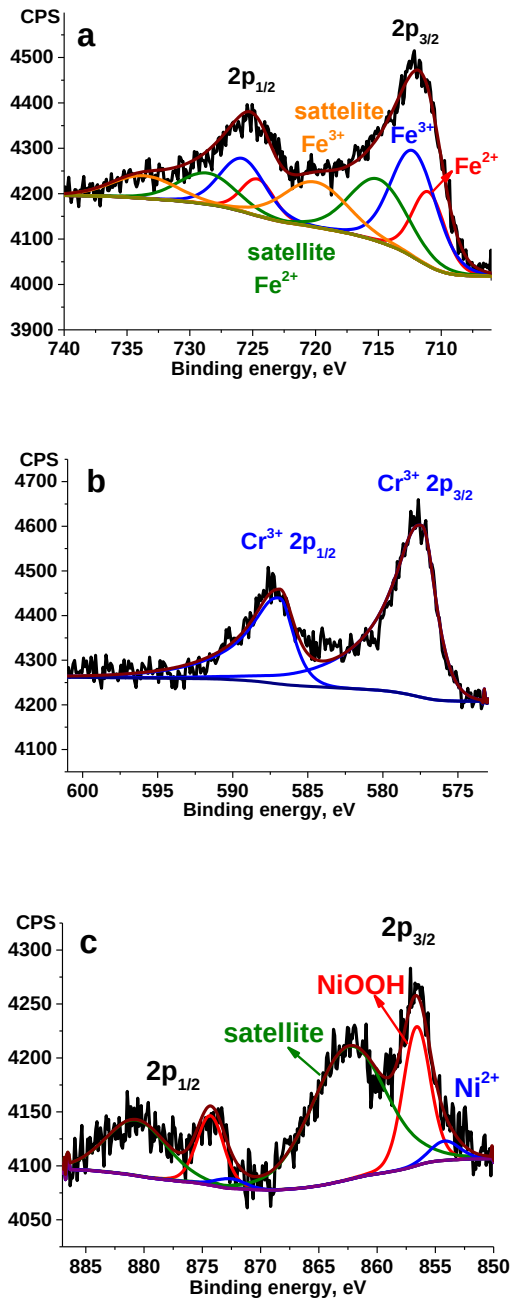

Figure S12. HR XPS of Fe 2p (a), Cr 2p (b) and Ni 2p (c) regions of SiO_2-Fe_3O_4-PPP-Cr-Ni.

Table S6. Fitting parameters for HR XPS of Fe 2p, Cr 2p and Ni 2p of SiO_2-Fe_3O_4-PPP-Cr-Ni.

Band	Position, eV	FWHM, eV	%Area
Fe			
1	711.00	3.06	11.69
2	712.20	4.26	23.37
3	715.00	5.43	17.49

4	720.03	6.06	14.12
5	724.60	3.06	5.84
6	725.80	4.26	11.69
7	728.60	5.43	8.74
8	733.63	6.06	7.06
Cr			
1	577.40	2.22	66.67
2	586.87	2.22	33.33
Ni			
1	854.20	3.00	2.89
2	856.60	2.75	19.01
3	862.43	7.54	49.97
4	872.60	3.00	1.44
5	874.31	2.75	9.50
6	880.65	6.19	17.18

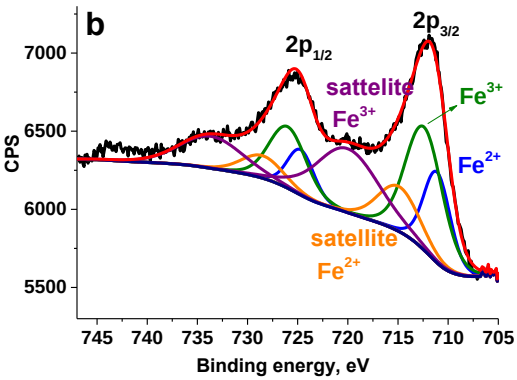

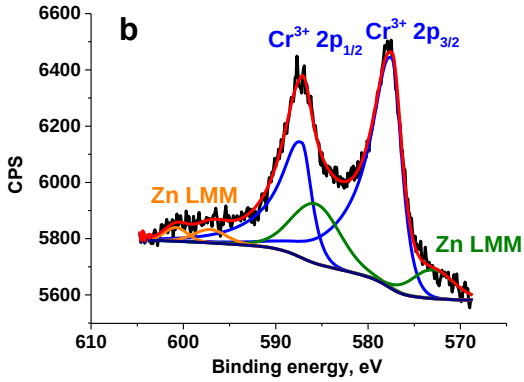

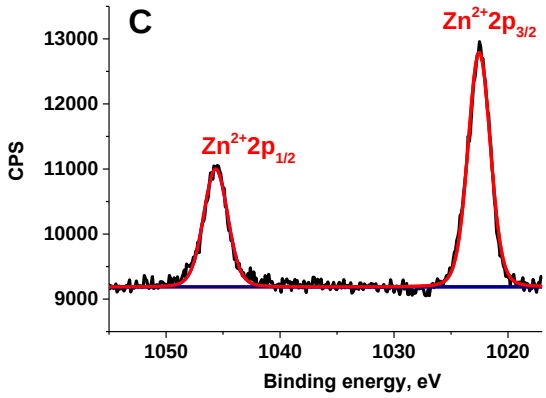

Figure S13. HR XPS of Fe 2p (a), Cr 2p (b) and Zn 2p (c) regions of Al_2O_3-Fe_3O_4-PPP-Cr-Zn.

Table S7. Fitting parameters for HR XPS of Fe 2p, Cr 2p and Zn 2p of Al_2O_3-Fe_3O_4-PPP-Cr-Zn.

Band	Position, eV	FWHM, eV	%Area
Fe			
1	711.11	3.12	12.54
2	724.71	3.12	6.27
3	712.40	4.35	23.65
4	726.00	4.35	11.83
5	714.93	4.89	9.74
6	728.53	4.89	4.87
7	720.05	7.33	20.74
8	733.65	7.33	10.37
Zn			
1	1022.53	2.30	64.66
2	1045.65	2.49	35.34
Cr			
1	577.42	2.56	49.08
2	587.18	2.56	24.54
3	573.00	5.28	6.56
4	585.64	6.12	15.75
5	600.80	2.91	1.71
6	597.09	4.11	2.37

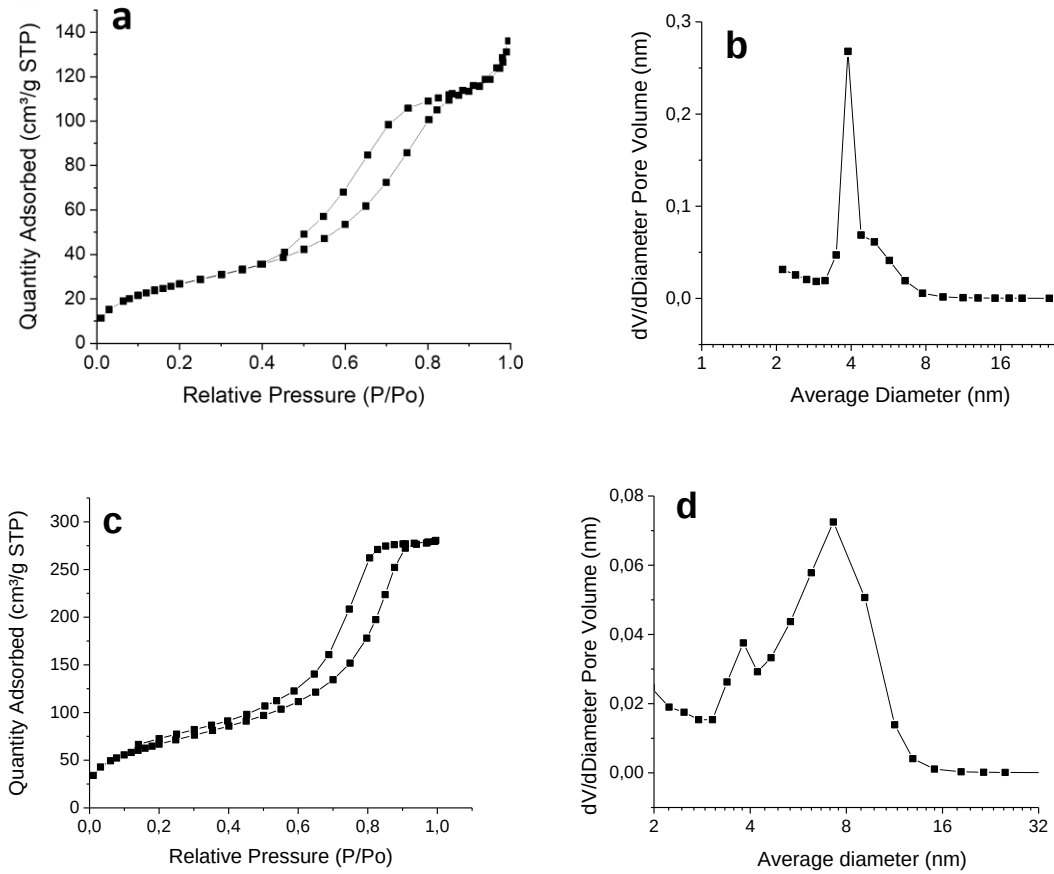

Figure S14. N_2 adsorption-desorption isotherms (a, c) and pore sizes distributions (b, d) of Al_2O_3-Fe_3O_4-PPP (a, c) and SiO_2-Fe_3O_4-PPP (c, d). **S_{BET}=164 m²/g** (Al_2O_3-Fe_3O_4-PPP) and **S_{BET}=246 m²/g** (SiO_2-Fe_3O_4-PPP).

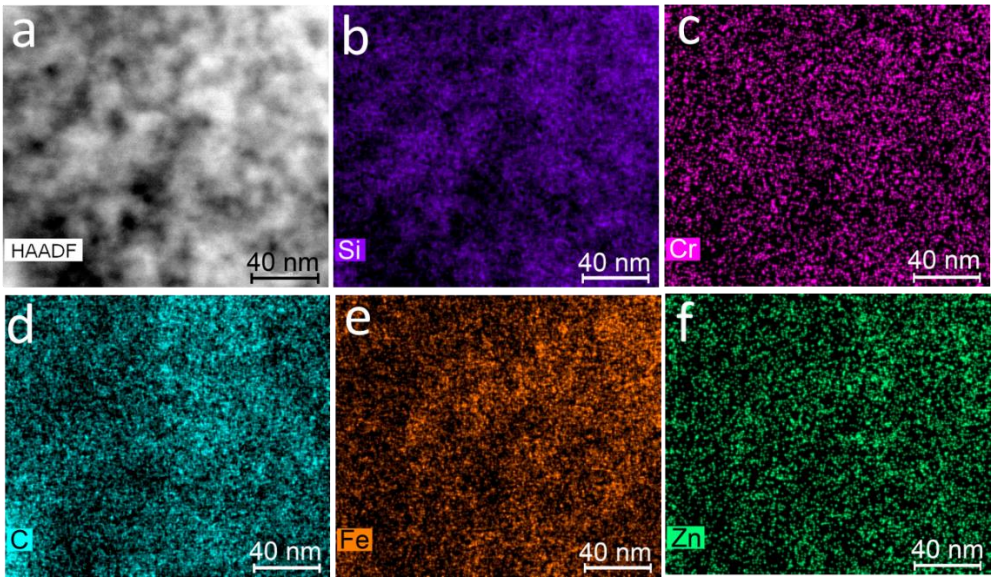

Figure S15. STEM dark field image (a) EDS maps of Si (b), Cr (c), C (d), Fe (e) and Zn (f) of SiO2-Fe3O4-PPP-Cr-Zn nanocomposite after catalysis.

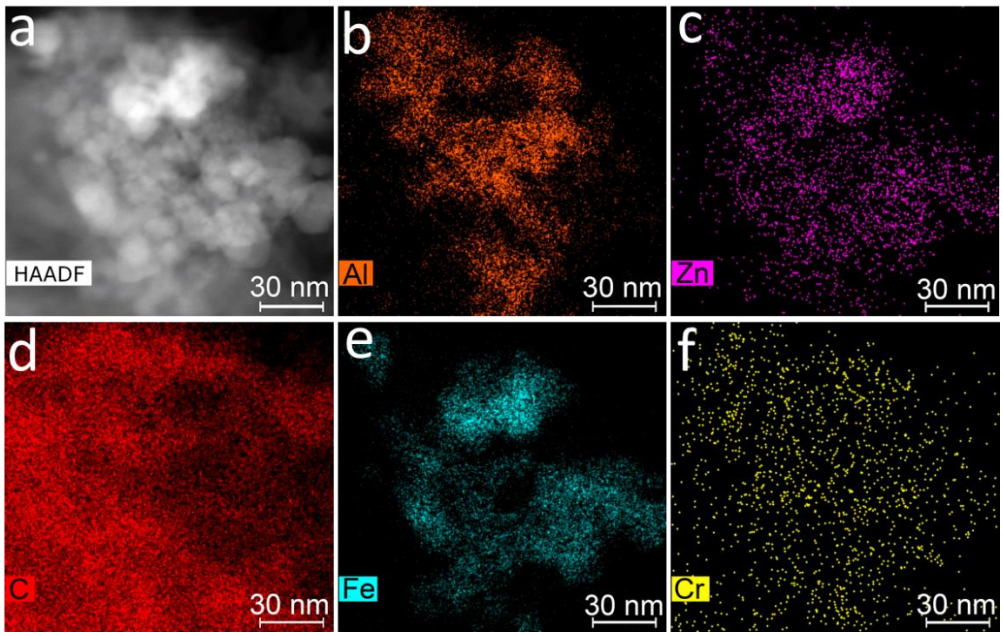

Figure S16. STEM dark field image (**a**) EDS maps of Al (**b**), Zn (**c**), C (**d**), Fe (**e**) and Cr (**f**) of Al_2O_3-Fe_3O_4-PPP-Cr-Zn nanocomposite after catalysis.

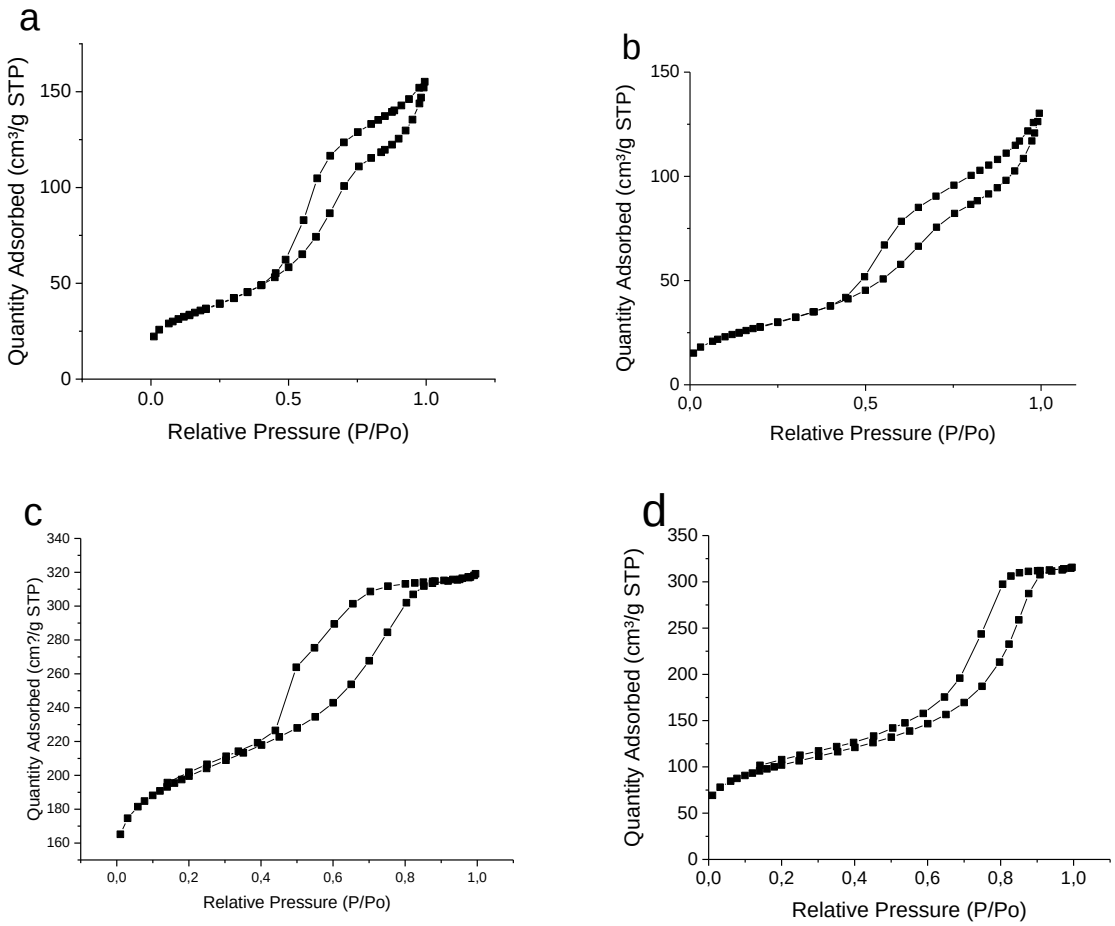

Figure S17. CO_2 adsorption-desorption isotherms SiO_2-Fe_3O_4 (a) (**S_{BET}=133 m^2/g)**, Al_2O_3-Fe_3O_4 (b) (**S_{BET}=103 m^2/g**), SiO_2-Fe_3O_4-PPP (c) (**S_{BET}=375 m^2/g**) and Al_2O_3-Fe_3O_4-PPP (d) (**S_{BET}=315 m^2/g)**.